Available online at www.sciencedirect.com
ScienceDirect
Ceramics International 36 (2010) 257–262
CERAMICS INTERNATIONAL
www.elsevier.com/locate/ceramint

Characterization of nanostructured ZnO produced by microwave irradiation

Titipun Thongtem [a,*], Anukorn Phuruangrat [b], Somchai Thongtem [b]

[a] Department of Chemistry, Faculty of Science, Chiang Mai University, Chiang Mai 50200, Thailand
[b] Department of Physics and Materials Science, Faculty of Science, Chiang Mai University, Chiang Mai 50200, Thailand

Received 9 February 2009; received in revised form 22 June 2009; accepted 26 July 2009
Available online 25 August 2009

Abstract

Different molar ratios of $Zn(NO_3)_2$ to NaOH were dissolved in de-ionized water, mixed to form solutions with different pH values and heated using 180 W microwave power (80 °C) in ambient atmosphere for 20 min. Wurtzite ZnO nanostructure was detected using an X-ray diffractometer (XRD) and a selected area electron diffraction (SAED) technique. The patterns were in accordance with those of the simulation. Scanning and transmission electron microscopes (SEM and TEM) revealed their nanostructures with different morphologies controlled by molar ratios of the starting agents as well as pH values of the solutions. High resolution transmission electron microscopic (HRTEM) technique shows that the crystallographic planes are aligned in lattice array. Seven different Raman wavenumbers at 334, 378, 410, 440, 541, 575 and 660 cm^{-1} were used to specify that the products were wurtzite structured ZnO. Photoluminescence (PL) spectra show their emission peaks at 385–394 nm due to the recombination process of free excitons.

Keywords: Microwave radiation; Wurtzite ZnO; Nanoparticles; Nanostructured flowers

1. Introduction

Recently, luminescent materials with different morphologies have become increasingly important. One of them is ZnO, which has a wide band gap (3.2 eV) and large exciton binding energy (60 meV) at room temperature [1,2]. It has a potential for using as light emitting diodes and diode lasers [3], transparent conducting electrodes of solar cells [4], and chemical and biological sensors [4]. The products with different morphologies were produced using a variety of methods such as single tetrapod-like nanostructure by catalyst-free rapid evaporation [5], maize-shaped micro-flowers by sonochemistry [6], single-crystalline tubes by a simple soft solution method [7], single-crystalline hexagonal prism nanorods by hydrothermal synthesis [8], nanodisks by a facile solvothermal method [9], fibers by sublimation method [10], nanowhisker clusters by wet chemical route [11], and nanorod arrays and branched microrods by aqueous solution route and rapid thermal processing [12].

In general, materials are classified into three groups concerning in their interaction with the microwave radiation: reflectors (bulk metals and alloys), transparencies (fused-silica and fluoropolymers), and absorbers (inorganic materials, powdered metals, metal oxides and metal halides) [13]. Thus microwave-assisted synthesis is appropriate for only microwave absorbing materials. When the radiation is supplied to solutions, one or more of their components is capable of coupling with it. Vibrating electric field applied a force on charged particles which vibrated accordingly. It can lead to higher heating rate than that achieved by conventional method, and can solve the problems of temperature and concentration gradients. Subsequently, pure products were produced [14]. The present research is to investigate the influence of NaOH (pH values) on the morphologies of ZnO produced using a microwave radiation without any further calcination.

2. Experiment

The 0.005 mole $Zn(NO_3)_2$ and different moles of NaOH were separately dissolved in 100 ml de-ionized water each and mixed to form 200 ml mixtures (solutions). For the solutions of 1:1, 1:5, 1:7.5, 1:10 and 1:15 molar ratios, the pH values were 7.0, 12.8, 12.9, 13.1 and 13.2, respectively. By 30 min stirring,

* Corresponding author. Tel.: +66 53 943344; fax: +66 53 892277.
E-mail addresses: ttpthongtem@yahoo.com, ttpthongtem@hotmail.com (T. Thongtem).

0272-8842/$36.00
doi:10.1016/j.ceramint.2009.07.027

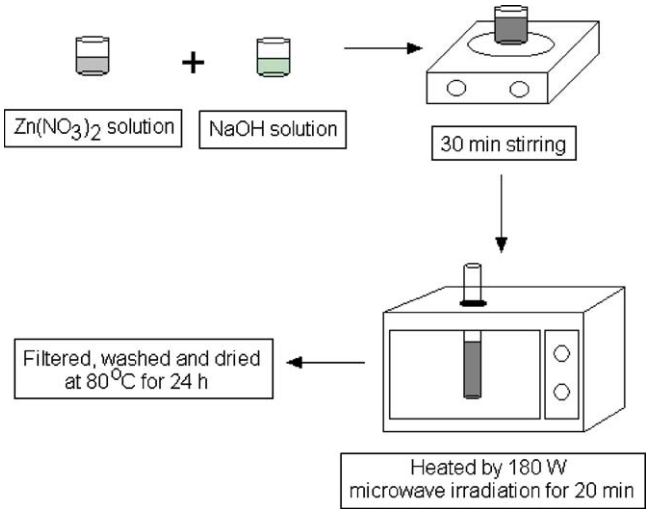

Fig. 1. Flow chart showing the process for the formation of ZnO.

these mixtures turned into white gels, which were subsequently heated up by 180 W microwave (2.45 GHz [15], multi-mode, 80 °C thermometer reading) in ambient atmosphere for 20 min (Fig. 1). The products were washed with water and ethanol, and dried at 80 °C for 24 h. They were characterized using an X-ray diffractometer (XRD) operated at 20 kV, 15 mA and using Cu Kα radiation with 0.1542 nm wavelength in the 2θ angular range of 15–60°, a transmission electron microscope (TEM) and a high resolution transmission electron microscope (HRTEM) as well as the use of the selected area electron diffraction (SAED) technique operated at 200 kV, a scanning electron microscope (SEM) operated at 15 kV and a Raman spectrometer using 50 mW Ar laser with 514.5 nm wavelength, and photoluminescence (PL) spectrometer using a 325 nm excitation wavelength at room temperature.

3. Results and discussion

XRD spectra of the products produced using different molar ratios of $Zn(NO_3)_2$ to NaOH are shown in Fig. 2. At 1:1 molar ratio (pH 7.0), XRD spectrum was rather broad. Its intensity was rather low, specifying that the product was composed of nanosized crystallites. The atoms were arranged in an array but they were not in perfect crystal lattice [16]. When 1:7.5 molar ratio (pH 12.9) was used in the process, the spectrum became sharper, and its intensity was higher. It became the sharpest and strongest at 1:15 molar ratio (pH 13.2). The degree or extent of product crystallinity was much improved. The atoms were arranged in crystal lattice. In general, pH values have the influence on the product morphologies, which will be explained latter in this section. Different morphologies seemed to play the role in the peak sharpness and height as well. Different peaks of XRD spectra were indexed using Bragg's law for diffraction. They corresponded to the (1 0 0), (0 0 2), (1 0 1), (1 0 2) and (1 1 0) planes of the JCPDS database with reference code 36–1451 [17]. The strongest intensity is at $2\theta = 36.3^\circ$ and diffracted from the (1 0 1) plane. The products were wurtzite structured ZnO (hcp) [4,6,17]. Intensity percents of the (0 0 2) peaks for

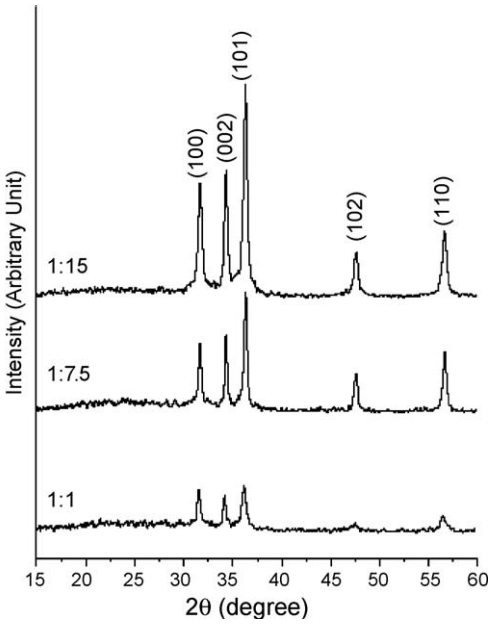

Fig. 2. XRD spectra of the products produced using different $Zn(NO_3)_2$ to NaOH molar ratio starting solutions.

1:7.5 and 1:15 molar ratios were higher than that shown in the JCPDS database. Their unit cells not only became the perfect crystals but also their growth was along the *c* axis [1]. Lattice parameters were calculated [18] and are shown in Table 1. They are very close to those of the corresponding JCPDS database [17]. The *c*/*a* ratios (more than one) supported the crystal growth along the *c* axis, and indicate the mobility of atoms in the solids. For the present research, no other impurities were detected although the products were produced under different conditions.

A definite existence of the products was analyzed using a Raman spectrometer. Test specimens are non-destructive and are able to re-use for other purposes. For wurtzite ZnO, there are totally 12 phonon modes, composing of one longitudinal-acoustic (LA), two transverse-acoustic (TA), three longitudinal optical (LO), and six transverse optical (TO) components [5]. The optical modes at the Γ point of Brillouin zone, predicted by group theory, are [5,12]

$$\Gamma_{\text{opt}} = 1A_1 + 2B_1 + 1E_1 + 2E_2 \quad (1)$$

The $2E_2$ modes are Raman active and non-polar. But for $1A_1$ and $1E_1$ modes, they are active for both Raman and infrared (IR). The $1A_1$ and $1E_1$ modes are polar and split into the LO and TO components. The $2B_1$ vibrations are silent modes. For the present research, three Raman spectra (Fig. 3) show seven

Table 1
Lattice parameters of ZnO produced using different $Zn(NO_3)_2$ to NaOH molar ratios and pH values.

$Zn(NO_3)_2$:NaOH (molar ratio)	pH	*a* (nm)	*c* (nm)	*c*/*a*
1:1	7.0	0.3253	0.5210	1.6016
1:7.5	12.9	0.3250	0.5213	1.6040
1:15	13.2	0.3232	0.5214	1.6132
JCPDS database [17]	–	0.3250	0.5207	1.6022

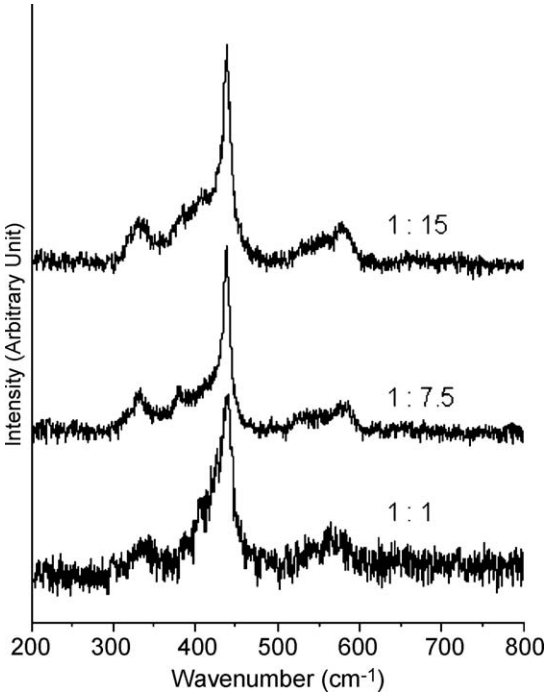

Fig. 3. Raman spectra of ZnO produced using different $Zn(NO_3)_2$ to NaOH molar ratio starting solutions.

bands with different vibration modes over the range 200–800 cm^{-1}. The bands with the same vibration modes of the three products are at the same wavenumbers. The high frequency mode (E_{2H}) [5,12], involved in only oxygen atoms [5], was clearly detected at 440 cm^{-1}. It was the strongest intensity, which is the common peak of wurtzite ZnO [4,12]. The low frequency mode (E_{2L} = 100 cm^{-1}) [12] was out of the range of the present analysis. The E_{1LO} mode of LO component at 575 cm^{-1} was due to the impurities and structural defects (oxygen vacancies and zinc interstitials) [12]. Two peaks corresponding to the ($E_{2H} - E_{2L}$) and A_{1TO} modes [4,12] were detected at 334 and 378 cm^{-1}, respectively. The ($E_{2H} - E_{2L}$) mode was the multiple-phonon scattering processes [4,12], and A_{1TO} mode the TO component [12,19]. Three peaks at 410, 541, and 660 cm^{-1} correspond to the E_{1TO} [5], A_{1LO} [5] and $2(E_{2H} - E_{2L})$, respectively. The spectra were specified that the products are ZnO (hcp) with wurtzite structure [6,12,19] and $P6_3mc$ space group [12,17]. These vibrations are in accordance with those of the four vibration modes at 331, 381, 437 and 582 cm^{-1} for ZnO nanostructure synthesized by a low-temperature solution process [4], seven vibration modes at 331, 381, 412, 437, 549, 583 and 664 cm^{-1} for single ZnO tetrapod-like nanostructure by catalyst-free rapid evaporation [5], and five vibration modes at 332, 382, 423, 438.22 and 586 cm^{-1} for as-grown ZnO nanorod arrays by aqueous solution route [12]. Their vibration frequencies are influenced by some parameters, such as atomic masses of Zn and O, and vibration constant of bonding between atoms in the lattice.

SEM, TEM and HRTEM images, and SAED and simulation patterns (Figs. 4 and 5) show that the products were successfully produced in a variety of shapes and sizes, influenced by different $Zn(NO_3)_2$ to NaOH molar ratios and basicity of the solutions. At 1:1 molar ratio, the product (Fig. 5a) was composed of nanoparticles in clusters. When more NaOH was added to be at 1:2.5 molar ratio, the product (result not shown) remained as nanoparticles in clusters. At the ratios of 1:5 (Fig. 4a) and 1:7.5 (Figs. 4b and 5d), the products were nanoplates in flower-like clusters. But for 1:10 (Fig. 4c) and 1:15 (Figs. 4d and 5f), they were composed of a number of spear-shaped particles in flower-like clusters. For comparison, flower-like clusters of spear-shaped particles produced by the present process are more perfect and beautiful than those produced by a surfactant-free and low-temperature process – ZnO flowers were composed of short, uneven and unformed nanorods [2], and low-temperature solution synthesis – ZnO nanostructure contained spear-shaped particles in flower-like clusters with a very fine thread woven across these particles [4]. Different molar ratios of the reactants can play the role in the solution properties. The amount of NaOH and pH values influenced the product morphologies, and the test temperature influenced the reaction rate. Comparing between SEM and TEM images, there is some difference between the two. The first shows three dimensional images of products, but the second shows only two dimensional images. For the same ratios, their morphologies are in good accordance, such as Figs. 4b and 5d, or 4d and 5f. Higher magnification TEM image of a spear-shaped particle produced using 1:15 molar ratio is shown in Fig. 5g. It grew along the [0 0 1] direction in the same manner as the XRD analysis. There were some defects containing in the particle. HRTEM image at a rectangle of Fig. 5g is shown in Fig. 5h. Parallel (0 0 2) planes composing of a number of atoms in crystal lattices were detected. They were the planes to which the growth or [0 0 1] direction was normal. The spear-shaped particle has a surface that is uneven. SAED pattern of the product produced using 1:1 molar ratio (Fig. 5b) was interpreted [20]. It appeared as a periodic array of bright spots showing that a number of atoms were arranged in their crystal lattices. The pattern shows the character of single crystal. These crystallographic planes correspond to ZnO (hcp) [17]. During the analysis, electron beam was in the [0 0 1] direction (zone axis). It was the direction that electrons were sent to the crystal facet. It is worth noting that bright spots of the pattern were arranged as hexagonal rings having the same center. These rings correspond to the basal plane of hcp unit cell. A diffraction pattern with the [0 0 1] zone axis was simulated (Fig. 5c) [21]. The simulated spots with the specified crystallographic planes are in the periodic array. Both the interpreted and simulated patterns are in good accordance. The a^*, b^* and c^* lattice vectors are in the [1 0 0], [0 1 0] and [0 0 1] directions, respectively. For one crystal structure, the corresponding lattice vectors are the same although their zone axes are different. At 1:15 molar ratio, SAED pattern (Fig. 5i) was interpreted [20]. It was composed of a periodic array of bright spots which is different from the previous one. At the present stage, the electron beam with the $[\bar{1}\,1\,0]$ direction was used in the process. The pattern also corresponds to ZnO (hcp) [17]. Additional concentric rings were detected. They were caused by the C grid. A diffraction pattern with the $[\bar{1}\,1\,0]$ zone axis was simulated (Fig. 5j) [21], and was in accordance with that of the

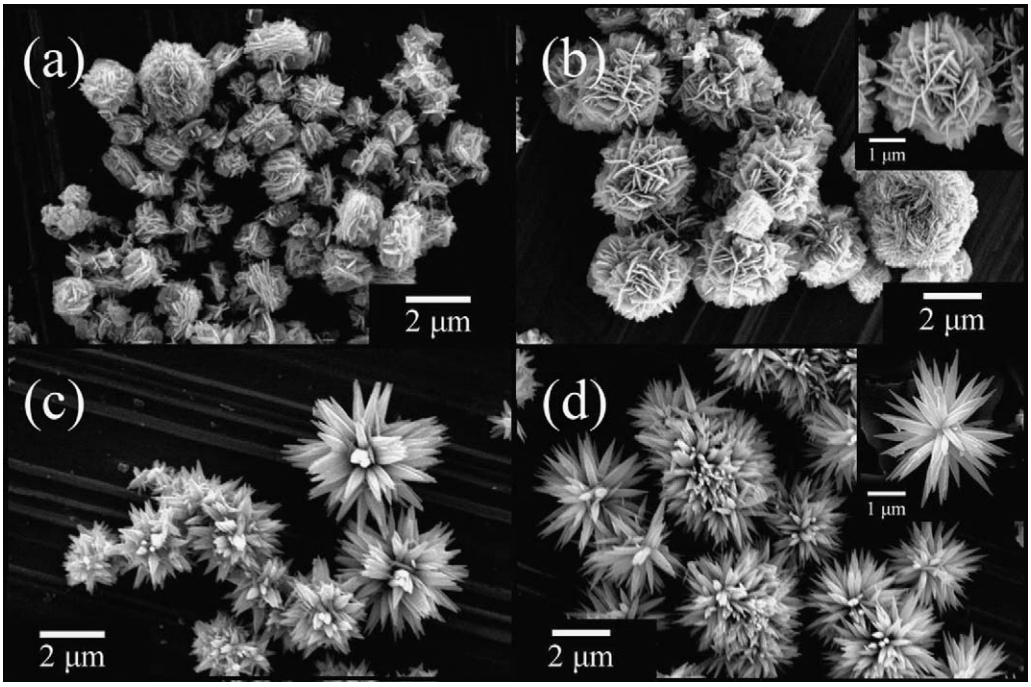

Fig. 4. SEM images of ZnO produced using $Zn(NO_3)_2$ to NaOH molar ratios of (a) 1:5, (b) 1:7.5, (c) 1:10 and (d) 1:15 starting solutions.

interpretation. At 1:7.5 molar ratio, the SAED pattern (Fig. 5e) was composed of concentric rings of bright spots. They show the character of polycrystalline. Electron beam diffracts from the crystallographic planes of the unit cells composing the product. The interpreted pattern [20,22] corresponded to the (1 0 0), (0 0 2), (1 0 1), (1 0 2), (1 1 0), (1 0 3), (1 1 2) and (2 0 1) planes. They were specified that the product was ZnO (hcp) [17].

To produce ZnO with different morphologies, OH^- ions were introduced into Zn^{2+} aqueous solutions, and $Zn(OH)_2$ colloid formed [1].

$$Zn^{2+} + 2OH^- \rightarrow Zn(OH)_2 \quad (2)$$

Some of $Zn(OH)_2$ colloid also dissolved into Zn^{2+} and OH^- ions [1].

$$Zn(OH)_2 \rightarrow Zn^{2+} + 2OH^- \quad (3)$$

The dissolving process proceeded until the concentrations of Zn^{2+} and OH^- attained the supersaturation values. At the present stage, ZnO nuclei started to form [1].

$$Zn^{2+} + 2OH^- \rightarrow ZnO + H_2O \quad (4)$$

At the same time, some $Zn(OH)_2$ of reaction (2) also reacted with OH^- ions to form $[Zn(OH)_4]^{2-}$ growth units [1].

$$Zn(OH)_2 + 2OH^- \rightarrow [Zn(OH)_4]^{2-} \quad (5)$$

Numbers of ZnO nuclei with their active sites and $[Zn(OH)_4]^{2-}$ growth units were controlled by basicity of the solutions [2,3]. Due to the concentration gradient in the solutions, $[Zn(OH)_4]^{2-}$ growth units diffused towards the nearby ZnO nuclei and adsorbed on active sites of the nuclei to produce particles with different morphologies, which were influenced by the nucleation, crystal growth rates and distribution of active sites. At 1:1 and 1:2.5 molar ratios, a number of ZnO nuclei were produced. They gradually grew into nanoparticles, and coalesced into clusters. At the present stages, they were assumed that active sites on ZnO nuclei to be many and growth rate of $[Zn(OH)_4]^{2-}$ units in the solutions to be low [2,3]. The units had very less chance to adsorb on the active sites. Hence, anisotropic growth was prohibited. Growths in all directions are almost at the same rates. Active sites and growth units were increased with the increase in the NaOH moles. At 1:5 and 1:7.5 molar ratios, the numbers of active sites and growth units were not sufficient to form spear-shaped particles [1–3]. Hence, nanoplates in flower-like clusters were produced. It is worth noting that the product was composed of flower-like clusters with different sizes. This shows that the clusters originated at random. Their growth rates, controlled by the diffusion of growth units, were also different. When more NaOH was added to be 1:10 molar ratio, numbers of the active sites and growth units were high enough to form spear-shaped particles in flower-like clusters. The central parts of the clusters were produced from ZnO nuclei [3]. At 1:15 molar ratio, numbers of active sites and growth units were higher, and spear-shaped particles in flower-like clusters became more perfect. Sharp ends of the spear-shaped particles were caused by the difference in growth rates of the crystallographic planes. Growth rates (R) of different planes are $R(0\,0\,1) > R(\bar{1}\,0\,\bar{1}) > R(\bar{1}\,0\,0) > R(\bar{1}\,0\,1) > R(0\,0\,\bar{1})$ [1,3]. For the (0 0 1) plane, its growth rate is the most rapid. Hence, the (0 0 1) plane faded away, and the (spear-shaped) particles were sharpened at the end of the c axis [1,3]. At the opposite end, growth rate of the $(0\,0\,\bar{1})$ plane is the slowest and its end has plain shape. The results were in accordance with other researchers [1–3].

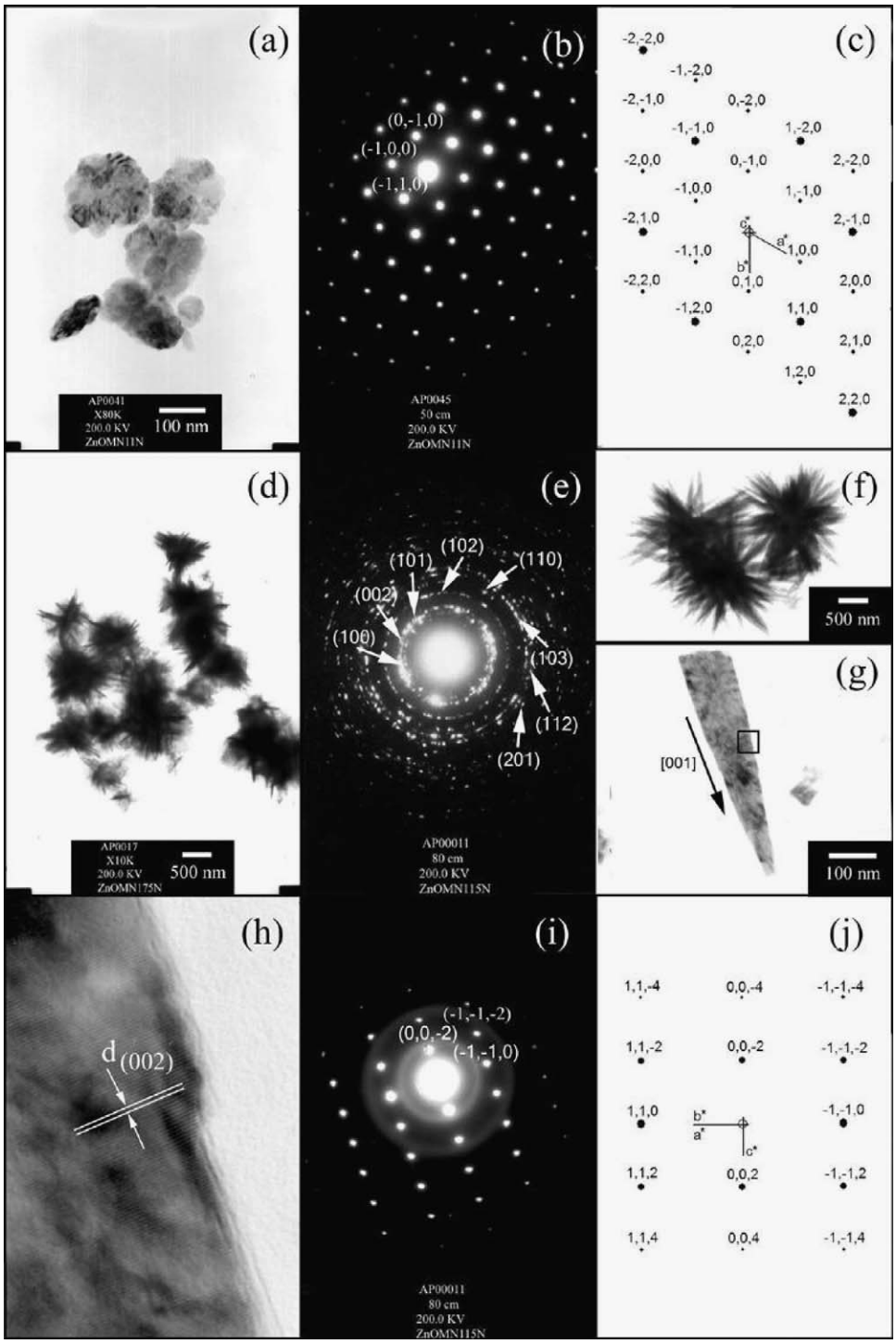

Fig. 5. TEM and HRTEM images, and SAED and simulation patterns of the products produced using different $Zn(NO_3)_2$ to NaOH molar ratio starting solutions. (a–c) 1:1, (d, e) 1:7.5, and (f–j) 1:15.

Photoluminescence (PL) spectra (Fig. 6) with the excitation wavelength of 325 nm show very strong peaks with their surrounding shoulders. The emission peaks are in the UV near band edge spectral region at 385–394 nm due to the recombination of free excitons of the products [2,6,23]. They are in accordance with a strong peak at 393 nm of flower-like ZnO nanostructure prepared by a surfactant-free and low-temperature process at a pH of 7.5, 8.5 and 10 [2], a strong UV emission at 384 nm of ZnO nanostructured flowers by low-temperature synthesis in a solution containing polyethylene glycol (PEG) at a pH of 7.5 [6], and an intensive UV emission at 389 nm of ZnO microspheres by a hydrothermal process [23]. PL intensity is controlled by the number of charged transfers. They were increased with the increase in the $Zn(NO_3)_2$ to NaOH molar ratios and basicity of the solutions, and are the highest for the product (spear-shaped particles in flower-like

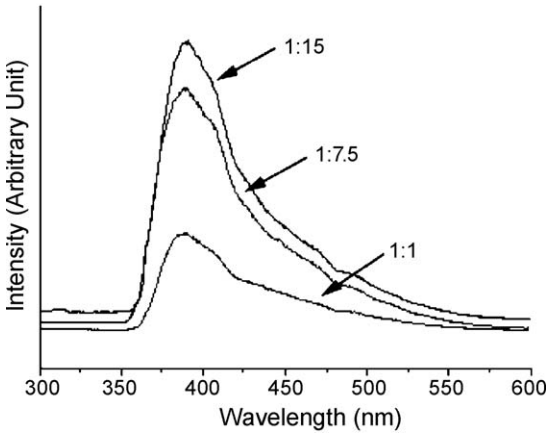

Fig. 6. PL spectra of ZnO produced using different $Zn(NO_3)_2$ to NaOH molar ratio starting solutions.

clusters) produced using 1:15 molar ratio of $Zn(NO_3)_2$ to NaOH, in the solution with a pH of 13.2. Shape and size of the crystals can play role in their emission as well. The surrounding shoulders were caused by the transition process relating to defects [2].

4. Conclusions

Nanostructured ZnO with different morphologies was successfully produced from different molar ratios of $Zn(NO_3)_2$ to NaOH by using a microwave radiation in ambient atmosphere. XRD, SAED and Raman analyses revealed the presence of wurtzite structured ZnO with the strongest Raman intensity at 440 cm^{-1}. Nanoparticles in clusters, nanoplates in flower-like clusters, and spear-shaped particles in flower-like clusters were characterized using SEM and TEM. They were influenced by molar ratios of the starting agents as well as pH values of the solutions. Photoluminescence (PL) spectra with 325 nm excitation wavelength show the strong emission peaks over the range of UV near band edge spectral region at 385–394 nm, due to the recombination of free excitons in the products.

Acknowledgement

The research was supported under the National Research University Project for Chiang Mai University, by the Commission on Higher Education, Ministry of Education, Thailand.

References

[1] H. Zhang, D. Yang, Y. Ji, X. Ma, J. Xu, D. Que, J. Phys. Chem. B 108 (2004) 3955.
[2] J. Liu, X. Huang, Y. Li, J. Duan, H. Ai, Mater. Chem. Phys. 98 (2006) 523.
[3] H. Zhang, D. Yang, X. Ma, Y. Ji, J. Xu, D. Que, Nanotechnology 15 (2004) 622.
[4] R. Wahab, S.G. Ansari, Y.S. Kim, H.K. Seo, G.S. Kim, G. Khang, H.S. Shin, Mater. Res. Bull. 42 (2007) 1640.
[5] S.H. Huang, Z. Chen, X.C. Shen, Z.Q. Zhu, K. Yu, Solid State Commun. 145 (2008) 418.
[6] J. Liu, X. Huang, Y. Li, J. Duan, H. Ai, L. Ren, Mater. Sci. Eng. B 127 (2006) 85.
[7] D. Wu, L. Huang, Q. Wang, X. Zhao, A. Li, Y. Chen, N. Ming, Mater. Chem. Phys. 96 (2006) 51.
[8] Y. Wang, M. Li, Mater. Lett. 60 (2006) 266.
[9] D. Chu, Y. Zeng, D. Jiang, Mater. Res. Bull. 42 (2007) 814.
[10] T. Shishido, K. Yubuta, T. Sato, A. Nomura, J. Ye, K. Haga, J. Alloys Compd. 439 (2007) 227.
[11] P. Jiang, J.J. Zhou, H.F. Fang, C.Y. Wang, S.S. Xie, Mater. Lett. 60 (2006) 2516.
[12] O. Lupan, L. Chow, G. Chai, B. Roldan, A. Naitabdi, A. Schulte, H. Heinrich, Mater. Sci. Eng. B 145 (2007) 57.
[13] J.W. Lekse, A.M. Pischera, J.A. Aitken, Mater. Res. Bull. 42 (2007) 395.
[14] C. Gabriel, S. Gabriel, E.H. Grant, B.S.J. Halstead, D.M.P. Mingos, Chem. Soc. Rev. 27 (1998) 213.
[15] S. Bhunia, D.N. Bose, J. Cryst. Growth 186 (1998) 535.
[16] C. Wu, X. Qiao, L. Luo, H. Li, Mater. Res. Bull. 43 (2008) 1883.
[17] Powder Diffract. File, JCPDS-ICDD, 12 Campus Boulevard, Newtown Square, PA 19073-3273, U.S.A., 2001.
[18] T. Thongtem, A. Phuruangrat, S. Thongtem, Mater. Lett. 61 (2007) 3235.
[19] D. Vernardou, G. Kenanakis, S. Couris, E. Koudoumas, E. Kymakis, N. Katsarakis, Thin Solid Film 515 (2007) 8764.
[20] T. Thongtem, A. Phuruangrat, S. Thongtem, Mater. Lett. 62 (2008) 454.
[21] C. Boudias, D. Monceau, CaRIne Crystallography 3.1, DIVERGENT S.A., Centre de Transfert, 60200 Compiègne, France, 1989–1998.
[22] T. Thongtem, S. Kaowphong, S. Thongtem, J. Mater. Sci. 42 (2007) 3923.
[23] H. Niu, Q. Yang, K. Tang, Y. Xie, F. Yu, J. Mater. Sci. 41 (2006) 5784.